

(*p,n*) Reaction on Deformed Nuclei Mg²⁵ and Mg²⁶†

C. WONG, J. D. ANDERSON, J. W. McCLURE, AND B. POHL

Lawrence Radiation Laboratory, University of California, Livermore, California

(Received 14 November 1966)

The Mg²⁵(*p,n*)Al²⁵ and Mg²⁶(*p,n*)Al²⁶ reactions to individual levels have been investigated to assess the applicability of a strong-coupling deformed isospin model in describing the “inelastic” (*p,n*) charge-exchange reaction. For nuclei in the rotational region, the model predicts a simple splitting of the quadrupole strength [obtained from the 0⁺ → 2⁺, Δ*T*=0, Mg²⁶(*p,n*) transition] among the members of the *K*= $\frac{5}{2}$ ground-state band in the Mg²⁵(*p,n*)Al²⁵ reaction. The measured cross section, excitation function, and angular distribution for the $\frac{5}{2}^+ \rightarrow \frac{7}{2}^+$ transition in Mg²⁵(*p,n*) are in fair agreement with the predictions of the deformed isospin model. The evidence for a quadrupole contribution to the $\frac{5}{2}^+$ ground state and $\frac{9}{2}^+$ excited state in Mg²⁵(*p,n*) is inconclusive because of the presence of a large contribution to the cross section from spin-flip with charge exchange. As in a previous experiment, the measured 0⁺ → 2⁺, Δ*T*=0 cross section is much larger than the theoretical prediction of the deformed isospin optical model. However, the 0⁺ → 2⁺ (*p,n'*) cross sections are correlated with the analogous 0⁺ → 2⁺ (*p,p'*) cross sections. In the Mg²⁶(*p,n*)Al²⁶ reaction, the measured 0⁺ → 2⁺, Δ*T*=0 cross section is three times the 0⁺ → 0⁺ isobaric cross section. On the other hand, the 0⁺ → 0⁺, Δ*T*=0; 0⁺ → 1⁺, 0⁺ → 3⁺, and 0⁺ → 5⁺, Δ*T*=1 cross sections are comparable, indicating that charge exchange with spin-flip and with Δ*l*=0, 2, 4 are almost as important as monopole charge exchange in the Mg²⁵(*p,n*)Al²⁵ reaction. The observation of *K*= $\frac{5}{2}$ to *K*= $\frac{1}{2}$ band transitions, which are comparable to *K*= $\frac{5}{2}$ to *K*= $\frac{5}{2}$ transitions in Mg²⁵(*p,n*), would seem to indicate that single-particle transitions are relatively more important when compared with the analogous (*p,p'*) scattering, and thus that an appreciable fraction of the *K*= $\frac{5}{2}$ to *K*= $\frac{5}{2}$ (*J*^π= $\frac{7}{2}^+$ or $\frac{9}{2}^+$) transition strength goes via single-particle matrix elements. It is concluded that a microscopic strong-coupling calculation, in which the charge-exchange part of the two-body interaction includes spin-flip and angular-momentum transfers up to Δ*l*=4, is needed to explain the measurements.

I. INTRODUCTION

IT is well known^{1,2} that the introduction of a quadrupole distortion in the real potential can explain the strong inelastic scattering to low-lying 2⁺ collective levels. It is also known³⁻⁵ that the inclusion of an isospin term in the optical potential can account for the (*p,n*) isobaric reaction. Satchler *et al.*⁵ therefore proposed that by deforming the isospin potential and using the strong-coupling model, one might explain the (*p,n'*) strengths to various collective levels in rotational nuclei. Figure 1 depicts graphically the predictions of the deformed isospin model with strong coupling as applied to Mg²⁵ and Mg²⁶. The total quadrupole (*p,n*) strength is given by the 0⁺ to 2⁺ (Δ*T*=0) transition in Mg²⁶(*p,n*). In Mg²⁵(*p,n*) this quadrupole strength is distributed among the $\frac{5}{2}^+$, $\frac{7}{2}^+$, and $\frac{9}{2}^+$ members of the *K*= $\frac{5}{2}$ band in the ratio of 5/14, 10/21, and 1/6. The corresponding contributions to the cross sections are 5/28, 10/42, and 1/12 of the 0⁺ → 2⁺ cross section, the factor of 0.5 arising from the difference in neutron excesses in Mg²⁵ and Mg²⁶ (see Sec. IV). Because of the quadrupole (Δ*l*=2) contribution to the Mg²⁵(*p,n*) ground-state reaction, the isobaric transitions should show different angular

distributions for Mg²⁵ and Mg²⁶. The (*p,n*) cross sections to the above-mentioned levels were therefore measured and compared with the predictions of the deformed isospin model. The (*p,n*) cross sections to other levels [5⁺, 3⁺, 1⁺, and unresolved doublet at ~1.80 MeV in Al²⁶ and $\frac{1}{2}^+$, $\frac{3}{2}^+$, $\frac{5}{2}^+$ (*K*= $\frac{1}{2}$ band) in Al²⁵] were also measured. The Al²⁷(*p,n*) isobaric reaction was also investigated and compared with the Mg²⁵(*p,n*) reaction. Since the neutron excess is the same for Mg²⁵ and Al²⁷, a comparison of total cross sections and angular distributions may also yield information on the magnitude of the quadrupole (Δ*l*=2) contribution to the Mg²⁵(*p,n*) reaction.

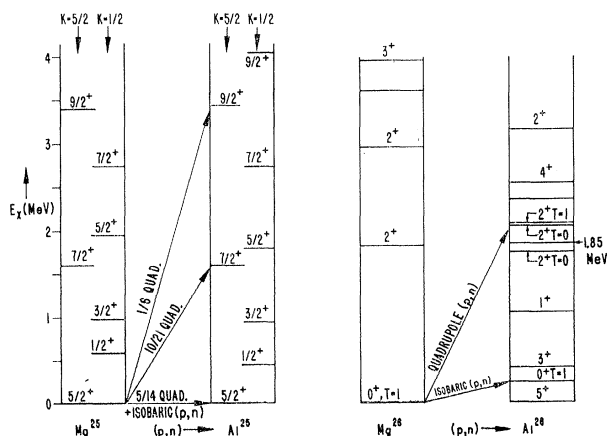


FIG. 1. Graphical illustration of the predictions of the deformed isospin model. The quadrupole strength obtained from the Mg²⁶(*p,n*) 0⁺ → 2⁺ transition is distributed among the *K*= $\frac{5}{2}$ band members in Mg²⁵(*p,n*).

† Work performed under the auspices of the U. S. Atomic Energy Commission.

¹ R. H. Bassel, G. R. Satchler, R. M. Drisko, and E. Rost, Phys. Rev. **128**, 2693 (1962).

² P. H. Stelson, R. L. Robinson, H. J. Kim, J. Rapaport, and G. R. Satchler, Nucl. Phys. **68**, 97 (1965).

³ A. M. Lane, Nucl. Phys. **35**, 676 (1962).

⁴ J. D. Anderson, C. Wong, J. W. McClure, and B. D. Walker, Phys. Rev. **136**, B118 (1964).

⁵ G. R. Satchler, R. M. Drisko, and R. H. Bassel, Phys. Rev. **136**, B637 (1964).

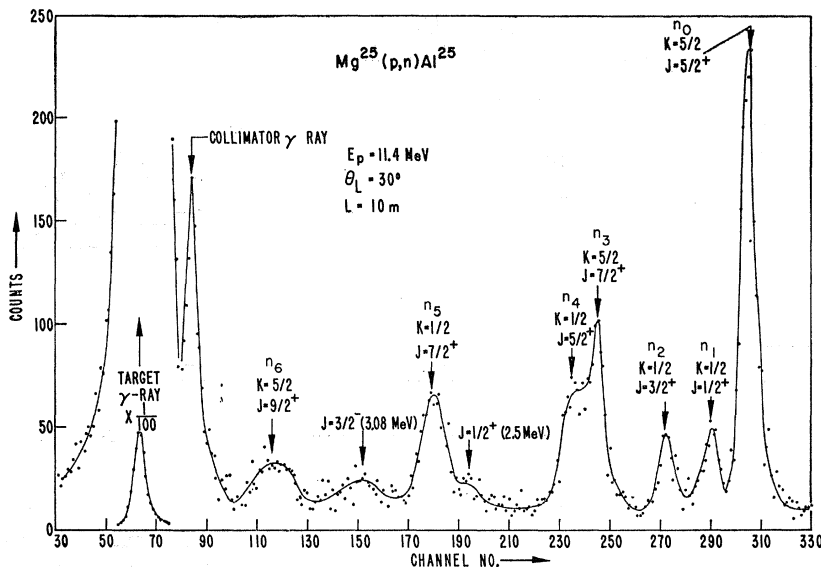


FIG. 4. Time-of-flight spectrum for $Mg^{25}(p,n)Al^{25}$ at a laboratory angle of 30° and bombarding energy of 11.4 MeV. n_0 , n_3 , and n_6 denote neutron groups leading to the $K=\frac{5}{2}$ band members in Al^{25} ; n_1 , n_2 , n_4 , n_5 denote groups leading to the $K=\frac{3}{2}$ band members in Al^{25} .

mg/cm² for the Mg^{25} and 2.0 ± 0.1 mg/cm² for the Mg^{26} targets. The variation of the thickness over the $\frac{1}{2}$ -in.-diam beam spot was less than $\pm 10\%$. At the proton energies utilized in this experiment, the Mylar produces no background neutrons. The aluminum target was a self-supporting 3-mg/cm²-thick metal foil of excellent uniformity. The thickness varied by less than $\pm 2\%$ over the $\frac{1}{2}$ -in.-diam beam-spot position. The beam traverses the thin self-supporting targets and is collected in a 6-in. Faraday cup located some 15 ft from the target. To suppress secondary electron emission from the target and Faraday cup, a negatively biased grid was inserted between target and Faraday cup.

D. Detector Efficiency

The detection efficiency of the 2-in. \times 2-in. pilot B plastic scintillator was calculated and then measured using the known cross sections for the production of $D(d,n)He^3$ neutrons. The calculated and measured efficiencies agreed within 5%. The cross sections have been corrected for the attenuation of the neutrons in 10 m of air, typically a 7 to 10% correction for 3- to 10-MeV neutrons.

III. EXPERIMENTAL RESULTS

Figure 4 shows a typical time-of-flight spectrum for $Mg^{25}(p,n)$ at a laboratory angle of 30° and bombarding energy of 11.4 MeV. The neutron groups leading to the $K=\frac{5}{2}$ and $K=\frac{3}{2}$ band members in Al^{25} are indicated⁸ by arrows. The remaining two peaks at channels 155 and 195 represent neutron groups leading to the lowest member of an odd-parity band and to the ground state

of another $K=\frac{3}{2}$ band, respectively. Angular distributions as a function of bombarding energy were measured for the neutron groups labeled n_0 , n_1 , n_2 , n_3 , n_4 , and n_6 . These distributions are displayed in Figs. 5, 6, and 7. The extraction of counts for n_3 and n_4 could be done reliably since the positions and line shapes are known. Neutron "group" n_5 included contributions from three or four close-lying levels and hence was ignored. The $\frac{3}{2}^-$ (3.08) and $\frac{1}{2}^+$ (2.5) groups were also ignored, since statistically significant cross sections could not be obtained because of the low intensities. The angular distributions were fitted by an expansion in terms of Legendre polynomials. From the zero-order coefficient in this expansion, the integrated cross sections of Table I were obtained. The number of neutron groups observed is dependent upon the bombarding energy and the neutron detector bias. The bias employed for the Mg^{25} , Mg^{26} , and Al^{27} measurements was 340-keV electrons, which is equivalent to 1.6-MeV neutrons. Because of the rapid variation of efficiency with neutron energy below ~ 2 MeV, cross sections are presented for $E_n \gtrsim 2.0$ MeV.

Figure 8 displays a typical time-of-flight spectrum for $Mg^{26}(p,n)$ at a laboratory angle of 15° and bombarding energy of 9.3 MeV. The arrows identify the neutron groups leading to the ground (n_0) and various excited states of Al^{26} (see Fig. 1).⁸ Again, the triad n_0 , n_1 , n_2 could be decomposed reliably since the line shapes and positions are accurately known. Neutron groups n_4 and n_5 were not adequately resolved at the higher bombarding energies. Hence angular distributions are presented for the unresolved doublet $n_{4,5}$ leading to Al^{26} levels at 1.76 and 1.85 MeV. Similarly, $n_{6,7}$ denotes unresolved neutron groups leading to a narrow 2^+ doublet located at 2.07 and 2.08 MeV in

⁸ The level structures of Mg^{25} , Al^{25} , Mg^{26} , and Al^{26} are taken from P. M. Endt and C. Van Der Leun [Nucl. Phys. 34, 1 (1962)].

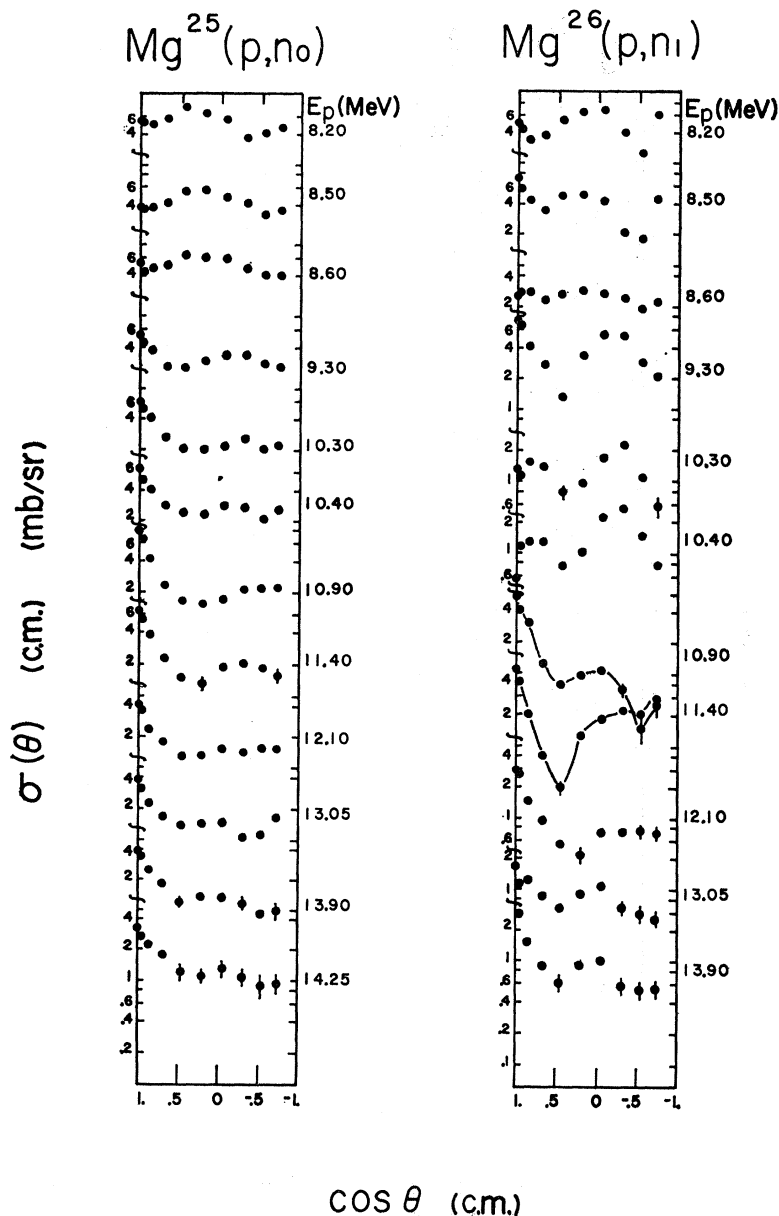


FIG. 5. Comparison of the (p, n) isobaric transition in Mg^{25} and Mg^{26} . The angular distributions are plotted in the order of increasing bombarding energy.

Al^{26} .^{9,10} The total (p, n) quadrupole strength is given by the transition to the $T=1$ member of this doublet, the 2.08-MeV level. Because of contributions from the 2.07 ($T=0$) level, $n_{6,7}$ yields an overestimate of the total quadrupole strength. In what follows, the assumption is made that $n_{6,7}$ yields the total $Mg^{26}(p, n)$ quadrupole strength since the 20% contamination from the $T=0$ level (estimated from $n_{4,5}$) does not materially affect the conclusions of this paper.

The angular distributions as a function of bombarding

energy for the various neutron groups are displayed in Figs. 5, 6, 9, and 10. Integrated cross sections are presented in Table II. The total cross sections presented in Tables I and II are plotted in Figs. 11–14.

IV. DEFORMED ISOSPIN MODEL-THEORY

Since deformed potentials have been treated extensively in many places^{1,2,5} only the salient features will be presented, noting in particular how the results are altered by the inclusion of isospin. Following Lane,³ the optical-model potential is of the form

$$U = U_0(r) + U_1(r)/A (\mathbf{t} \cdot \mathbf{T}_0), \quad (1)$$

⁹ R. W. Kavanagh, W. R. Mills, and R. Sherr, Phys. Rev. **97**, 248L (1955).

¹⁰ L. L. Green, J. J. Singh, and J. C. Willmott, Proc. Phys. Soc. (London) **A69**, 335 (1956).

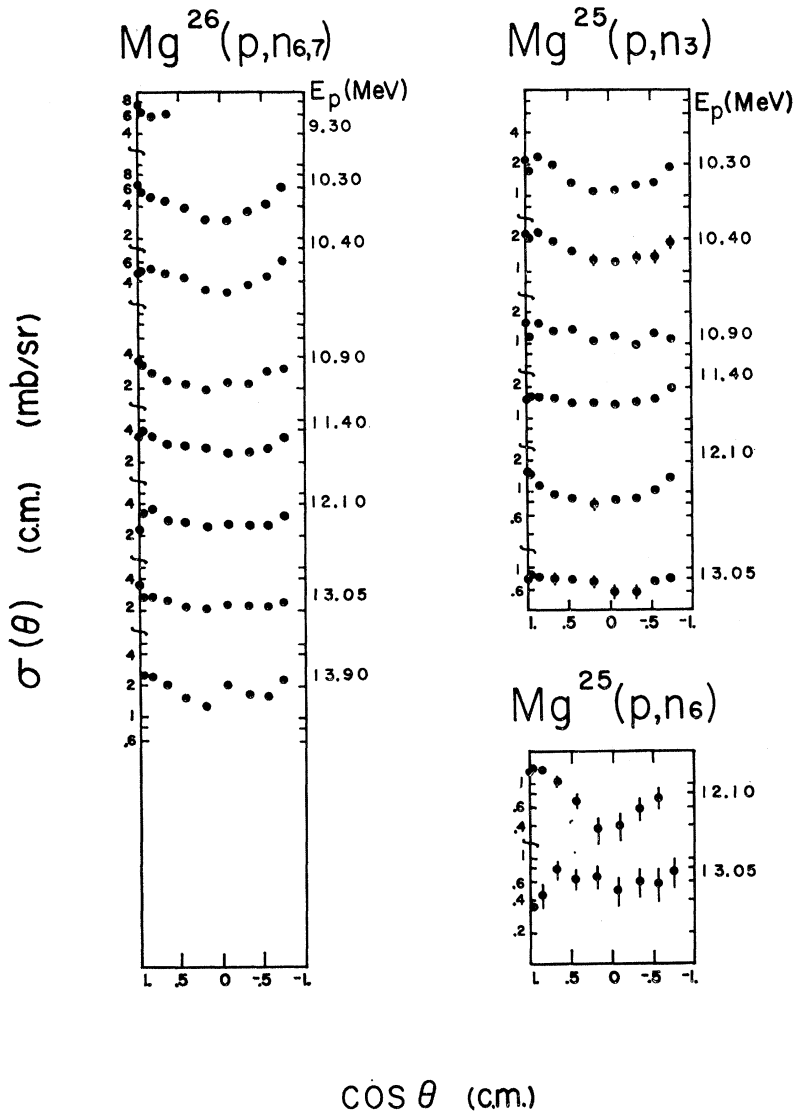


FIG. 6. Angular distributions as a function of bombarding energy for the quadrupole transition in $Mg^{26}(p,n)$ and the $K = \frac{5}{2}$ band transitions in $Mg^{25}(p,n)$. $Mg^{25}(p,n_3)$ and $Mg^{25}(p,n_6)$ represent transitions to the $J^\pi = \frac{7}{2}^+$, $K = \frac{5}{2}$, and $J^\pi = \frac{9}{2}^+$, $K = \frac{5}{2}$ levels of Al^{26} , respectively.

where \mathbf{t} is the isospin of the projectile, \mathbf{T}_0 is the isospin of the target, and A is the mass number of the target. Following Satchler *et al.*⁵ the nuclear surface is allowed

to be nonspherical, so that

$$R(\theta, \phi) = R_0 \left[1 + \sum_{l,m} \alpha_{l,m} Y_l^m(\theta, \phi) \right], \quad (2)$$

TABLE I. Integrated cross sections σ_l (in mb) for $Mg^{25}(p,n)Al^{26}$. Errors shown are relative errors. The absolute cross-section scale is uncertain to $\pm 5\%$.

E_p	n_0	n_1	n_2	n_3	n_4	$n_{3,4}$	n_6
8.20	68 ± 3	13.2 ± 1	12 ± 5				
8.50	55 ± 2	11.6 ± 1	10 ± 4				
8.60	63 ± 3	14 ± 1	13 ± 2				
9.30	38.5 ± 2	7.7 ± 0.5	11 ± 1				
10.30	32 ± 2	8.8 ± 0.5	10.4 ± 1	20 ± 2	17 ± 1		
10.40	34 ± 2	9.1 ± 0.5	11.2 ± 0.5	20 ± 0.5	20 ± 1		
10.90	29 ± 2	6.4 ± 0.5	7.1 ± 0.5	14.8 ± 1	12.6 ± 0.5		
11.40	25.2 ± 2	5.7 ± 0.5	6.7 ± 0.5	19.6 ± 0.5	13 ± 1		
12.10	21 ± 1	4.3 ± 0.5	5.2 ± 0.5	12.7 ± 0.5	7.2 ± 0.5		10.4 ± 1
13.05	20 ± 1	4.1 ± 0.5	4.1 ± 0.25	9.4 ± 0.5	8.6 ± 0.5		8.2 ± 1
13.90	18 ± 1					15.0 ± 1	
14.25	16.5 ± 1					12.3 ± 1	

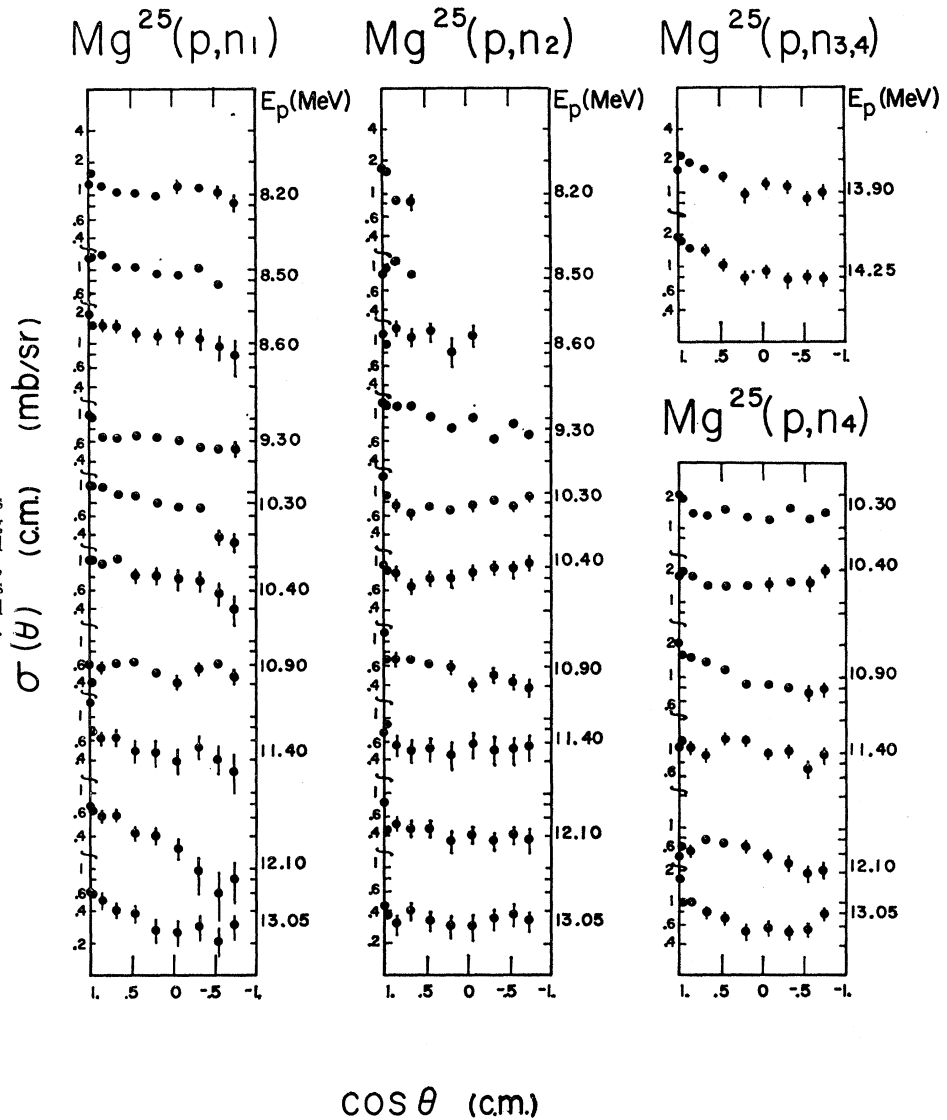


FIG. 7. Angular distributions as a function of bombarding energy for the $K = \frac{1}{2}$ band transitions in $Mg^{25}(p, n)$. n_1, n_2 , and n_4 are the neutron groups leading to the $J^\pi = \frac{1}{2}^+, \frac{3}{2}^+$, and $\frac{5}{2}^+, K = \frac{1}{2}$ band members in Al^{26} .

where the $\alpha_{l,m}$'s are the 2^l -pole deformation parameters. Expanding the isospin potential in powers of α and keeping only the first-order terms yields

$$\frac{U_1(r, \theta, \phi)}{A} (\mathbf{t} \cdot \mathbf{T}_0) = V_1 \frac{(\mathbf{t} \cdot \mathbf{T}_0)}{A} \times \left[f(x) - \frac{R_0}{a} \sum_{l,m} \alpha_{l,m} Y_l^m(\theta, \phi) \frac{df(x)}{dx} \right], \quad (3)$$

where $f(x)$ is the form factor for the volume isospin potential, $x = (r - R_0)/a$ and a is the Woods-Saxon diffuseness parameter. The first term of Eq. (3) gives rise to the quasielastic (p, n) reaction while the second term can induce the quasi-inelastic $0^+ \rightarrow 2^+(p, n')$ transition. For (p, p') , $U_0(r)$ is expanded in a manner identical to (3), the only difference being that $V_1(\mathbf{t} \cdot \mathbf{T}_0)/A$ is

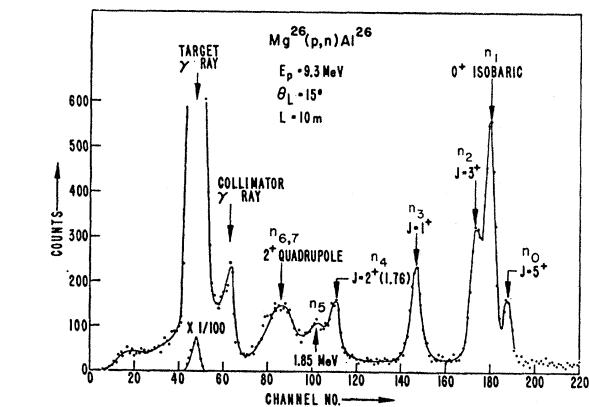


FIG. 8. Time-of-flight spectrum for $Mg^{26}(p, n)Al^{26}$ at a laboratory angle of 15° and bombarding energy of 9.3 MeV. The neutron groups leading to levels in Al^{26} are indicated by arrows.

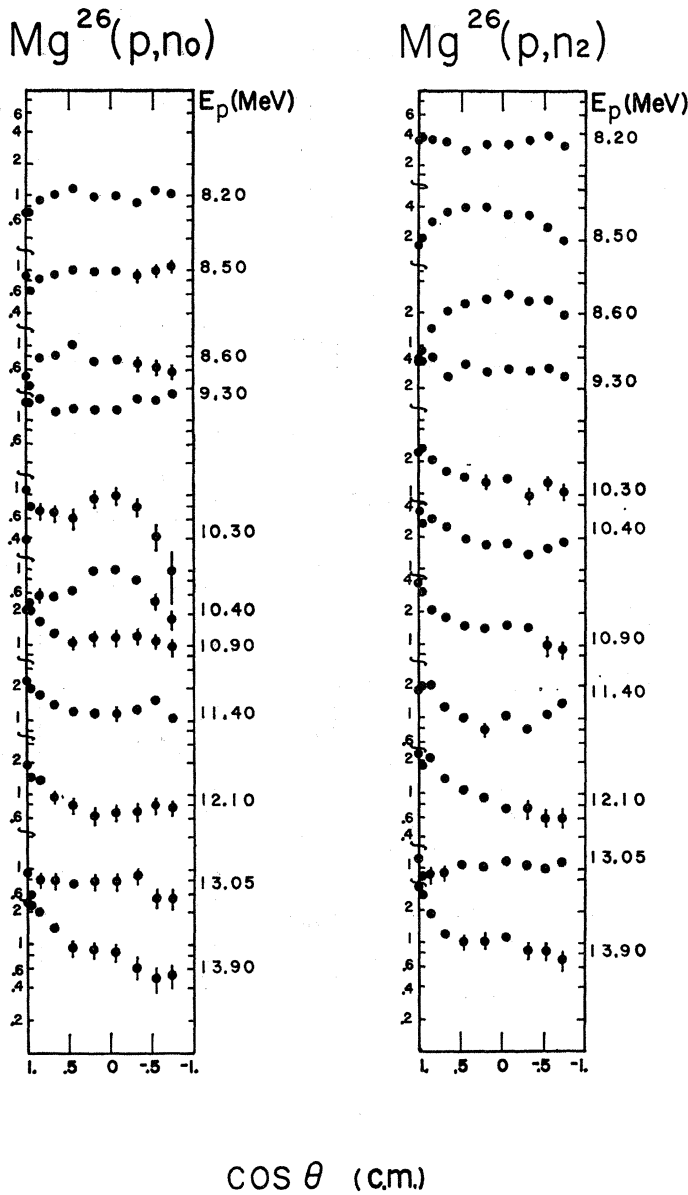


FIG. 9. Angular distributions as a function of bombarding energy for $Mg^{26}(p, n_0)$ and $Mg^{26}(p, n_2)$; n_0 is the neutron group leading to the $Al^{26} J^\pi = 5^+$ ground state while n_2 is the neutron group leading to the $Al^{26} J^\pi = 3^+$ second excited state.

replaced by V_0 , the depth of the real potential. Since $(\mathbf{t} \cdot \mathbf{T}_0)$ operates only on the isospin part of the wave function yielding $\frac{1}{2}(N-Z)^{1/2}$, it is easy to see that in

the adiabatic limit and neglecting Coulomb effects,

$$\frac{\sigma(p, n')}{p, p\sigma'} = \frac{1}{4}(N-Z) \left(\frac{V_1}{V_0 A} \right)^2 \left(\frac{k_n}{k_p} \right), \quad (4)$$

TABLE II. Integrated cross sections σ_i (in mb) for $Mg^{26}(p, n)Al^{26}$. Errors shown are relative errors. The absolute cross-section scale is uncertain to $\pm 5\%$.

E_p (MeV)	n_0	n_1	n_2	n_3	$n_{4,5}$	$n_{6,7}$
8.2	12.1 ± 1	74 ± 4	40 ± 4	40 ± 6		
8.5	8.8 ± 1	32 ± 2	28.6 ± 2	46 ± 8		
8.6	12.1 ± 1	56 ± 3	38.5 ± 2	32 ± 2		
9.3	17.9 ± 1	44 ± 5	38.5 ± 3	31 ± 2	55 ± 11	71 ± 13
10.3	8.1 ± 0.5	14.8 ± 2	17 ± 1	18.4 ± 1	33 ± 2	55 ± 2
10.4	8.3 ± 0.5	18.7 ± 2	24.2 ± 2	20.3 ± 2	40 ± 2	57 ± 3
10.9	14.8 ± 2	14.3 ± 2	18.1 ± 2	12.6 ± 1	25 ± 2	32 ± 1
11.4	15.8 ± 1	24.8 ± 2	15.4 ± 1	11.6 ± 1	23 ± 1	37 ± 2
12.1	10.1 ± 1	10.1 ± 5	12.1 ± 0.5	7.7 ± 0.5	21 ± 1	35 ± 2
13.05	8.6 ± 0.5	10.4 ± 1	13.2 ± 0.5	8.0 ± 0.5	15.4 ± 1	29 ± 2
13.90	11.8 ± 1	11.3 ± 1	13.7 ± 0.5	7.8 ± 0.5	11.3 ± 0.5	25 ± 2

provided the deformation parameters and form factors are identical for the ordinary optical and isospin potentials. The terms k_n and k_p are the wave numbers of the emitted neutron and proton, respectively. Equation (4) can be used to predict the (p, n') cross section if the corresponding (p, p') measurements are available without recourse to detailed DWBA (distorted-wave Born approximation) calculations.⁵

Since there is strong coupling between the odd-nucleon hole and a permanently deformed even-even core, the quasi-inelastic cross section within the

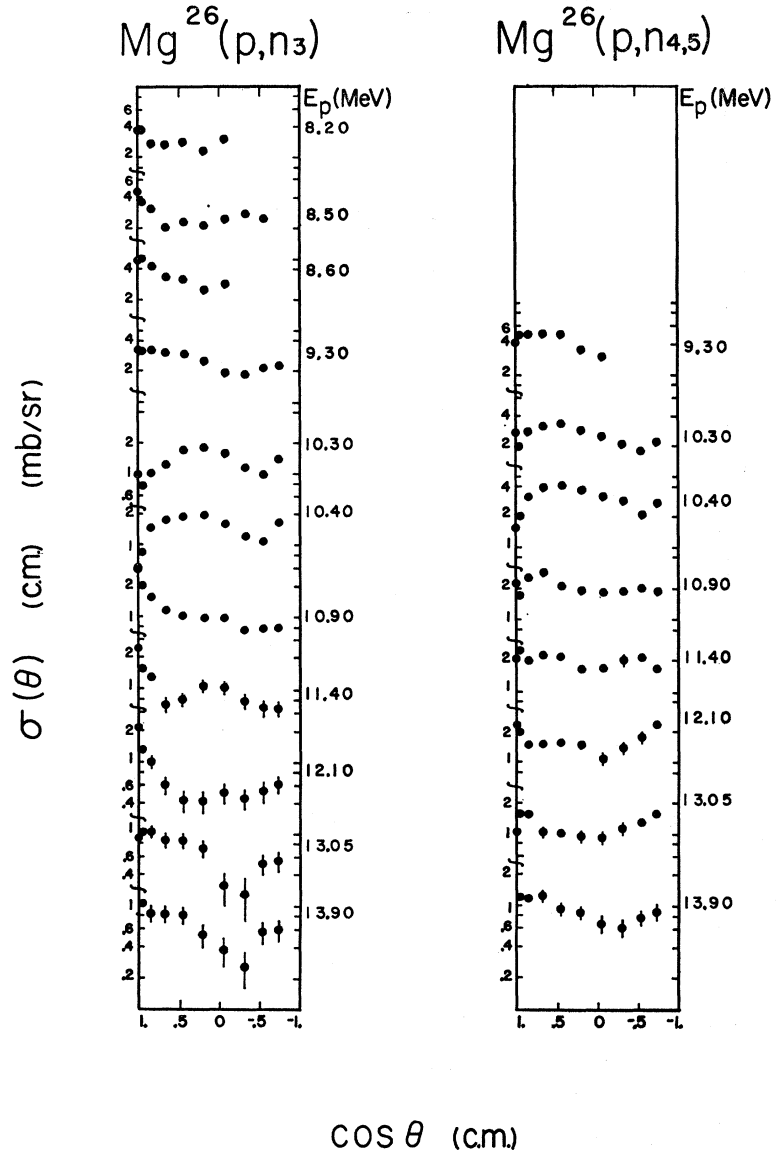


FIG. 10. Angular distributions as a function of bombarding energy for the 0⁺ to 1⁺ transition [Mg²⁶(p,n₃)] and for the 0⁺ to unresolved doublet at approximately 1.8-MeV excitation energy in Al²⁶ [Mg²⁶(p,n_{4,5})].

ground-state band in the odd-mass nucleus is related to the even-mass nucleus cross section by

$$\frac{d\sigma}{d\Omega}(J, K \rightarrow J', K) = \frac{(N-Z)_J}{(N-Z)_0} \sum_l \langle J, l, K, 0 | J', K \rangle^2 \times \frac{d\sigma}{d\Omega}(0 \rightarrow l), \quad J \neq J', \quad l=2, 4, 6 \dots \quad (5)$$

The expression $J=J'$ yields the contribution of the deformed even-even core to the quasielastic cross section. The quasielastic cross section ($J=J'$) in the odd-mass nucleus is therefore given by

$$\frac{d\sigma}{d\Omega}(J, K \rightarrow J, K) = \frac{(N-Z)_J}{(N-Z)_0} \left[\frac{d\sigma}{d\Omega}(0 \rightarrow 0) + \sum_l \langle J, l, K, 0 | J, K \rangle^2 \frac{d\sigma}{d\Omega}(0 \rightarrow l) \right], \quad l=2, 4, 6 \dots \quad (6)$$

The terms $(N-Z)_J$ and $(N-Z)_0$ are the neutron excesses in the odd- and even-mass nucleus, respectively; and $d\sigma/d\Omega(0 \rightarrow 0)$ and $d\sigma/d\Omega(0 \rightarrow l)$ are, respectively, the monopole (isobaric) and l -pole cross section in the even-mass nucleus. Applying (5) and (6) to the magnesium isotopes and considering only the quadrupole term ($l=2$) yield

$$\frac{d\sigma}{d\Omega}\left(\frac{5}{2}, \frac{5}{2} \rightarrow \frac{5}{2}, \frac{5}{2}\right) = \frac{1}{2} \left[\frac{d\sigma}{d\Omega}(0 \rightarrow 0) + \frac{5}{14} \frac{d\sigma}{d\Omega}(0 \rightarrow 2) \right], \quad (7a)$$

$$\frac{d\sigma}{d\Omega}\left(\frac{5}{2}, \frac{5}{2} \rightarrow \frac{7}{2}, \frac{5}{2}\right) = \frac{1}{2} \left[\frac{10}{21} \frac{d\sigma}{d\Omega}(0 \rightarrow 2) \right], \quad (7b)$$

$$\frac{d\sigma}{d\Omega}\left(\frac{5}{2}, \frac{5}{2} \rightarrow \frac{9}{2}, \frac{5}{2}\right) = \frac{1}{2} \left[\frac{1}{6} \frac{d\sigma}{d\Omega}(0 \rightarrow 2) \right]. \quad (7c)$$

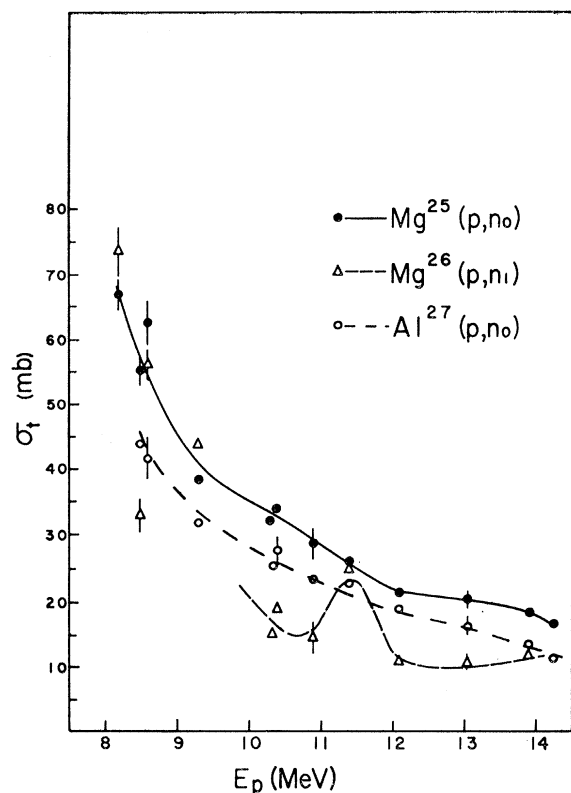


FIG. 11. Integrated cross sections as a function of bombarding energy for the (p,n) isobaric transition in Mg^{25} , Mg^{26} , and Al^{27} .

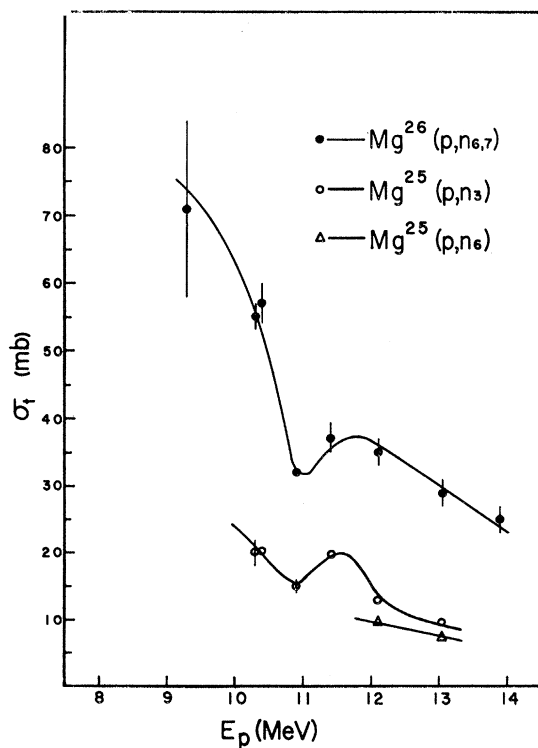


FIG. 12. Integrated cross sections as a function of bombarding energy for the quadrupole transition in $Mg^{26}(p,n)$ and the $K=3/2$ band transitions in $Mg^{25}(p,n)$.

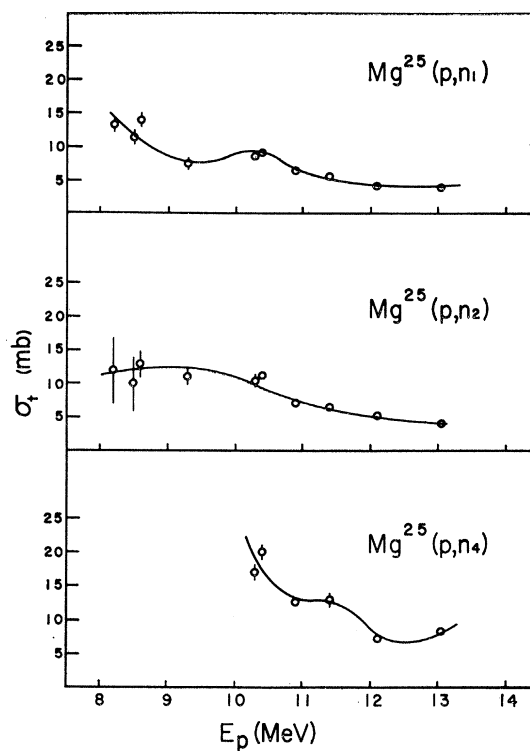


FIG. 13. Integrated cross sections as a function of bombarding energy for the $K=1/2$ band transitions in $Mg^{26}(p,n)$.

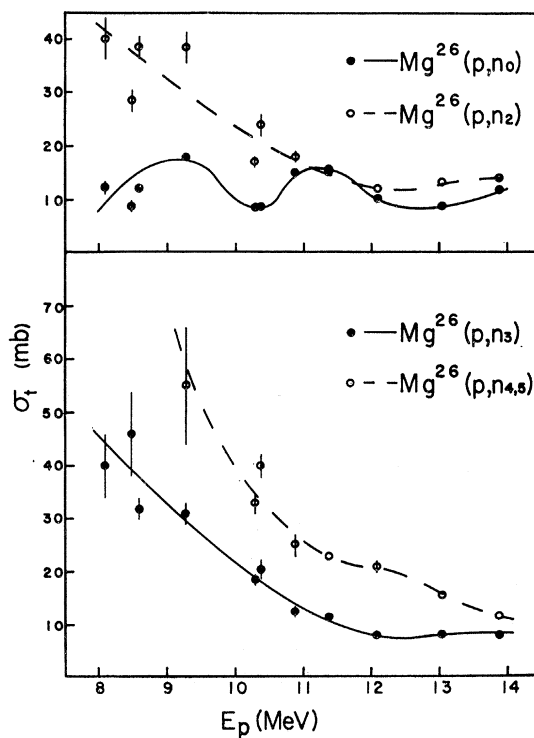


FIG. 14. Integrated cross sections as a function of bombarding energy for the remaining $Mg^{26}(p,n)$ transitions (i.e., excluding the isobaric and quadrupole transitions).

V. DISCUSSION

A. Isobaric Transition in Mg^{25} , Mg^{26} , and Al^{27}

The angular distributions for the isobaric transition in Mg^{25} , Mg^{26} , and Al^{27} are shown in Figs. 5 and 15, while the integrated cross sections are displayed in Fig. 11. The $Al^{27}(p, n_0)$ distributions, the $Mg^{25}(p, n_0)$ distributions above 9.3 MeV, and the $Mg^{26}(p, n_1)$ distributions above 10.9 MeV are all forward-peaked and all vary gradually with energy, in agreement with the assumed direct nature of the (p, n) isobaric reaction. The rapid change in the shape of the angular distributions in Mg^{25} and Mg^{26} at ~ 8.6 MeV and in Mg^{26} at ~ 10.3 MeV is attributed to the presence of intermediate structure resonances. The Mg^{26} isobaric distributions (Fig. 5) display more intermediate structure resonances; this fact is directly reflected in the more rapid fluctuation of the Mg^{26} integrated cross sections with energy (see Fig. 11). In contrast, the Mg^{25} and Al^{27} integrated cross sections show a monotonic decrease with increasing bombarding energy.

A comparison of the Mg^{25} and Mg^{26} isobaric reaction above 10.9 MeV shows the Mg^{25} distributions to be washed out compared to the Mg^{26} distributions. It is tempting to attribute this difference to the quadrupole contribution to the Mg^{25} isobaric reaction. Indeed, if one were to add incoherently 5/28 of the $0^+ \rightarrow 2^+$ distribution ($n_{6,7}$) to one-half of the Mg^{26} isobaric distribution [Eq. (7a)], the resulting predicted distributions for Mg^{25} agree well in shape with the measurements. However, the predicted cross sections are low by roughly 40%. This discrepancy could be attributed to

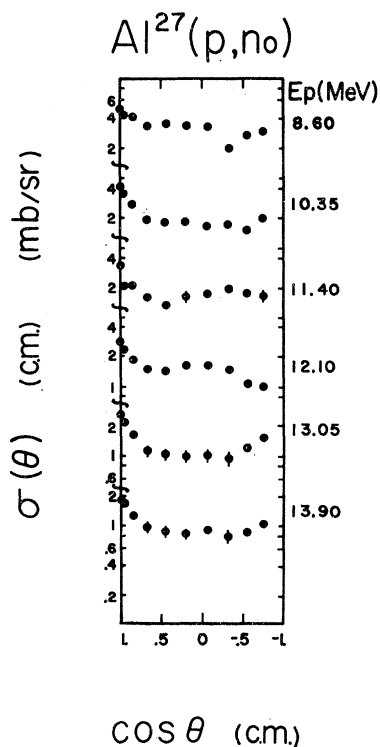


FIG. 15. Angular distributions as a function of bombarding energy for the isobaric transition in $Al^{27}(p, n)$.

TABLE III. Comparison of measured and calculated intensity ratios.

	Deformed isospin (quadrupole)	Measured ($E_p > 12$ MeV)
$\sigma(\frac{5}{2}^+ \rightarrow \frac{7}{2}^+)/\sigma(0^+ \rightarrow 2^+)$	10/42	$\sim \frac{1}{3}$
$\sigma(\frac{5}{2}^+ \rightarrow \frac{9}{2}^+)/\sigma(\frac{5}{2}^+ \rightarrow \frac{7}{2}^+)$	0.35	~ 0.8

the contribution from charge exchange with spin-flip which was ignored in the deformed isospin optical model and which is known to be important because of the sizable (p, n') cross sections to the 1^+ , 3^+ , and 5^+ levels in Al^{26} . Evidence for spin-flip in the p, n reaction on O^{18} and O^{17} ,¹¹ and the titanium isotopes¹² has been presented previously.

Since Al^{27} is presumably a $d_{5/2}$ proton hole weakly coupled to a vibrational Si^{28} core,¹³ the quadrupole transition cannot contribute to the Al^{27} isobaric reaction.⁵ Hence, assuming equal spin-flip contributions in Mg^{25} and Al^{27} , one would expect the Mg^{25} cross sections to be larger. This is observed experimentally: The Mg^{25} cross sections are higher by roughly 25%, which is in excellent agreement with the estimated quadrupole contribution. To see if the Mg^{25} , Mg^{26} , and Al^{27} isobaric cross sections are quantitatively consistent with the above description requires detailed calculations with the deformed isospin optical model generalized to include charge exchange with spin-flip.

B. Distribution of Quadrupole Strengths to $\frac{7}{2}^+$ and $\frac{9}{2}^+$ Levels in $Mg^{25}(p, n)Al^{25}$

Because of the contribution from charge exchange with spin-flip, one would not expect the cross sections to the $\frac{7}{2}^+$ and $\frac{9}{2}^+$ levels in $Mg^{25}(p, n)$ to be given by the deformed isospin model, i.e., Eqs. (7b) and (7c). This expectation is verified, as is shown in Table III. However, the close agreement between the predicted and measured ratio for the $\frac{5}{2}^+ \rightarrow \frac{7}{2}^+$ to $0^+ \rightarrow 2^+$ cross sections can be interpreted as a small contribution from charge exchange with spin-flip for the $\frac{5}{2}^+ \rightarrow \frac{7}{2}^+$ transition. As a consequence, the excitation functions and angular distributions should be crudely similar for the $0^+ \rightarrow 2^+$ and $\frac{5}{2}^+ \rightarrow \frac{7}{2}^+$ transitions. Figure 12 displays the excitation functions. The $(\frac{5}{2}^+ \rightarrow \frac{7}{2}^+)$ transition [$Mg^{25}(p, n_3)$] indeed displays crudely the same excitation-function shape as the $(0^+ \rightarrow 2^+)$ transition [$Mg^{26}(p, n_{6,7})$]. Figure 6 displays the angular distributions. Except at 12.1 and 10.9 MeV, the angular distributions of the $0^+ \rightarrow 2^+$ and $\frac{5}{2}^+ \rightarrow \frac{7}{2}^+$ transitions are very similar in shape. On the other hand, the $\frac{5}{2}^+ \rightarrow \frac{9}{2}^+$ transition contains only $\frac{1}{6}$ of the quadrupole strength. The measured cross-section ratio $[\sigma(\frac{5}{2}^+ \rightarrow \frac{9}{2}^+)/\sigma(\frac{5}{2}^+ \rightarrow \frac{7}{2}^+)]$ of ~ 0.8 compared to the pure quadrupole prediction of

¹¹ S. D. Bloom, J. D. Anderson, W. F. Hornyak, and C. Wong, Phys. Rev. Letters **15**, 264 (1965).

¹² C. D. Goodman, J. D. Anderson, and C. Wong, this issue, Phys. Rev. **156**, 1249 (1967).

¹³ G. M. Crawley and G. T. Garvey, Phys. Letters **19**, 228 (1965).

0.35 (see Table III) indicates that the $\frac{5}{2}^+ \rightarrow \frac{9}{2}^+$ transition contains sizable contributions from spin-flip and/or possibly from higher angular-momentum transfers, i.e. $\Delta l=4$. Hence, it is not surprising that the $\frac{5}{2}^+ \rightarrow \frac{9}{2}^+$ distributions [$\text{Mg}^{25}(p, n_6)$] are quite different in shape from the $0^+ \rightarrow 2^+$ distributions (see Fig. 6).

C. Magnitude of Predicted Quadrupole Transition

Using Eq. (4) with $V_1=100$ MeV,⁵ $V_0=50$ MeV and $\sigma(p, p')$ obtained from Schrank *et al.*¹⁴ the predicted $\text{Mg}^{26}(p, n')$ ($0^+ \rightarrow 2^+$) cross section is 0.15 mb. The measured value, obtained by extrapolation to 18 MeV, is ~ 15 mb, which is a factor of 100 larger than the prediction of the deformed isospin model. Application of Eq. (4) to O^{18} and Fe^{56} shows the measurements are similarly factors of 100 and 90 larger than the calculations, respectively. The $\text{Fe}^{56}(p, n')$ and $\text{Fe}^{56}(p, p')$ $0^+ \rightarrow 2^+$ measurements at 18 MeV were taken from Anderson *et al.*,⁴ and Eccles *et al.*,¹⁵ respectively; the $\text{O}^{18}(p, n')$ and $\text{O}^{18}(p, p')$ $0^+ \rightarrow 2^+$ measurements between 8–14 MeV were taken from Anderson *et al.*¹⁶ and Stevens *et al.*,¹⁷ respectively. Satchler *et al.*⁵ found from DWBA deformed-isospin-model calculations that the measured cross section in $\text{Fe}^{56}(p, n')$ $0^+ \rightarrow 2^+$ was a factor of 50 larger than prediction. This is to be compared with our value of 90 obtained from Eq. (4). The factor-of-2 discrepancy is mainly due to a difference in normalization since Satchler *et al.*⁵ normalized their calculation to the forward peak while use of Eq. (4) effectively normalizes to the total integrated cross section. It would appear that the deformed isospin model in the case of O^{18} , Mg^{26} , and Fe^{56} predicts the quadrupole cross section roughly two orders of magnitude smaller than the measurements. Alternatively, this implies that the effective β 's for (p, n') are an order of magnitude larger than the (p, p') β 's. Such a large effective β for (p, n') is unreasonable since it would imply an (n, n') β vastly different from the corresponding (p, p') β , in contradiction to the measurements of Stelson *et al.*² The O^{18} , Mg^{26} , and Fe^{56} results have shown that the equality sign in Eq. (4) should be replaced by a proportionality sign. In this context then, the $\sigma(p, n')$ cross sections are correlated with the corresponding $\sigma(p, p')$ cross sections.

D. Need for Microscopic Model

In the previous sections, it was shown that there was good evidence for a quadrupole contribution to the $\frac{5}{2}^+ \rightarrow \frac{7}{2}^+$ transition in $\text{Mg}^{25}(p, n)$. The evidence for a quadrupole contribution to the $\frac{5}{2}^+$ ground state and $\frac{9}{2}^+$

excited state in Al^{25} is inconclusive because of the sizable contribution to the cross section from charge exchange with spin-flip. Although correlated with $\sigma(p, p')$, the predicted quadrupole (p, n') cross sections are two orders of magnitude smaller than the measurements. The deformed isospin model is therefore in qualitative agreement with certain features of the data and yet in violent disagreement with others.

One may seriously question the adequacy of the deformed isospin model since the quadrupole transition in $\text{Mg}^{26}(p, n)$ and the $K=\frac{5}{2}$ band transitions in $\text{Mg}^{25}(p, n)$ are not greatly enhanced relative to the other transitions, as is the case with (p, p') . For example, in (p, n') the $0^+ \rightarrow 2^+$ transition is only three times larger than the other transitions while in (p, p') the corresponding enhancement is 30.¹⁴ Similarly, in $\text{Mg}^{25}(p, n)$ the $(\frac{5}{2}^+ \rightarrow \frac{7}{2}^+)$ $K=\frac{5}{2}$ band cross section is only a factor of two larger than the $(\frac{5}{2}^+ \rightarrow \frac{1}{2}^+)$ or $\frac{3}{2}^+)$ $K=\frac{1}{2}$ band cross sections. In contrast, in (p, p') experiments,¹⁴ the corresponding ratio is >10 . It would seem that a microscopic description¹⁸ is preferable since it would allow one to calculate all transitions to levels for which deformed shell-model wave functions are available and would allow one to include explicitly the spin dependence in the two-body force.

In $\text{Mg}^{26}(p, n)$ above the resonance region ($E_p > 12$ MeV), the $0^+ \rightarrow 2^+$ transition is roughly three times larger than the $0^+ \rightarrow 0^+$ isobaric transition. However, the $0^+ \rightarrow 0^+$, $0^+ \rightarrow 5^+$, $0^+ \rightarrow 3^+$, and $0^+ \rightarrow 1^+$ cross sections are all comparable, indicating that charge exchange with spin-flip and pure charge exchange are equally important components of the two-body force in the microscopic model. Inclusion of a charge exchange with spin-flip strength approximately equal to the pure charge-exchange strength in the two-body force can probably account¹⁹ for the comparable $0^+ \rightarrow 0^+$ and $0^+ \rightarrow 1^+$ ($\Delta T=1$, $\Delta l=0$) cross sections. However, the microscopic model,¹⁸ which does not include "knockout" or a tensor component in the two-body force, cannot account for the relatively large $0^+ \rightarrow 3^+$ ($\Delta T=1$, $\Delta l=2$ or 4 with spin-flip), $0^+ \rightarrow 5^+$ ($\Delta T=1$, $\Delta l=4$ or 6 with spin-flip) and $0^+ \rightarrow 2^+$ ($\Delta T=0$, $\Delta l=2$) cross sections since preliminary calculations^{16,19} have shown that the higher even-multipole transitions are much smaller than the monopole transition. Finally, the comparable $\text{Mg}^{26}(p, n)$ cross sections to the 0^+ , 1^+ , 3^+ , and 5^+ levels in Al^{26} would argue for the correctness of a direct-reaction description as opposed to a compound-nucleus-reaction description since the cross sections are not proportional to $(2J_f+1)$, where J_f is the spin of the final nucleus Al^{26} .

ACKNOWLEDGMENTS

The authors are indebted to Dr. A. Kerman, Dr. R. Lawson, and Dr. V. Madsen for helpful discussion.

¹⁴ G. Schrank, E. K. Warburton, and W. W. Daehnick, Phys. Rev. **127**, 2159 (1962).

¹⁵ S. F. Eccles, H. F. Lutz, and V. A. Madsen, Phys. Rev. **141**, 1067 (1966).

¹⁶ J. D. Anderson, S. D. Bloom, W. F. Hornyak, V. A. Madsen, and C. Wong (to be published).

¹⁷ J. Stevens, H. F. Lutz, and S. F. Eccles, Nucl. Phys. **76**, 129 (1966).

¹⁸ V. A. Madsen, Nucl. Phys. **80**, 177 (1966).

¹⁹ V. A. Madsen (private communication).